DYNAMIC CHARACTERISTICS OF SEMI-BONDED CARBON FIBER-REINFORCED ELASTOMERIC ISOLATOR (SB-CFREI)

Heshmatollah Adib NATANZI
Doctoral Candidate, The University of British Columbia, Canada
hojat.adib@civil.ubc.ca

Carlos E. VENTURA
Professor, The University of British Columbia, Canada
ventura@civil.ubc.ca

Solomon TESFAMARIAM
Associate Professor, The University of British Columbia, Canada
Solomon.Tesfamariam@ubc.ca

ABSTRACT: Over the past thirty years seismic isolation has been considered as a viable earthquake damage mitigation technique, and has been implemented to protect important new and existing structures. However, due to high production cost of the isolators, and implementation challenges of the conventional seismic isolators, application of this protective technology has been limited to important buildings. To ensure widespread application of the base isolation system, especially in developing countries, not only the production and implementation cost must be reduced, but the isolation efficiency and its effectiveness must improve as well. With this intention in mind, a new cost effective Elevated Semi-Bonded Carbon Fiber-Reinforced Elastomeric Isolator (ESB-CFREI) with higher isolation and implementation efficiency is being proposed by the authors. The innovative ESB-CFREI undergoes lateral cyclic excitations with a unique deformation mechanism that differs from that of conventional Bonded Steel Reinforced Elastomeric Isolators SREI and the Un-Bonded Carbon Fiber Reinforced Elastomeric Isolators UB-CFREI. The ESB-CFREI can be used in isolation as an independent "Component Isolator" or combined with other component Isolators to form a CESB-CFREI "Compound Isolator". Each component isolator has a different bonding value and, according to the experimental outcomes, each isolator has different effective lateral shear, axial compression stiffness, damping and dynamic characteristics.

In this paper by conducting a series of experimental test, the dynamic and mechanical characteristics of ESB-CFREI and the isolator's damping and isolation efficiency are investigated. The experimental program was conducted with dual shear configuration on 12 ESB-CFREI test specimens fabricated in 6 identical pairs. The experimental outcome also demonstrates the effect of bonding variation on dynamic characteristics, performance and efficiencies of the ESB-CFREI under combined compression and lateral cyclic loadings. The tests outcome is expected to promote the wide spread implementation of the innovative ESB-CFRE and CESB-CFREI as an efficient low-cost seismic Isolator.

1. Introduction

Increasing numbers of devastating earthquakes combined with unsafe construction practices are the predominant cause of human loss of life. The frequent occurrence of destructive earthquakes in the world with high magnitudes intensifies casualties and financial loss each year. For example in year 1990 occurrence of 18 earthquakes with magnitude 7 and greater [USGS National Earthquake Information Center] is alarming. In this same year only in Iran (Rudbar-Manjil 7.4) earthquake, the loss of life

exceeded 44000. Unfortunately, the high seismic zones of developing world are highly vulnerable and suffer the most. Low-rise, low-importance residential and commercial buildings are the typical buildings in developing regions that are most vulnerable to earthquake ground motions as they lack proper technical supervision during construction. These buildings are mostly characterized by a low fundamental period of vibration. To protect the buildings and reduce loss of life effectively, the application of innovative low cost seismic protection systems (e.g. base-isolation system, Naeim and Kelly 1999) should be considered as a possible viable option. The systems must be capable to de-tune and shift the natural frequency of these low- to medium-rise buildings away from the predominant ground motion frequency of earthquakes, thus leading to significant reduction of the seismic demand.

Kelly (1997, 1999) highlighted that the problem with adapting the seismic isolation to developing countries is that conventional isolators are large, expensive, and heavy. A single isolator can weigh up to 1 ton or more. To extend this valuable earthquake resistant strategy to housing and other public buildings, it is necessary to reduce the cost and weight of the isolators. Both the weight and cost of the isolators can be reduced by eliminating the steel reinforcing plates and replacing them with fiber reinforcement of high strength (Kelly 1999). Since 1999, many analytical and experimental studies have been conducted on Bonded and UN-Bonded Fiber-Reinforced Elastomeric Isolators (Kelly 1999, 2002; Moon et al. 2002; Kang et al. 2003; Ashkezaria et al. 2008; Mordini and Strauss 2008; Toopchi-Nehzad et al. 2009, 2011; Naghshineh et al. 2014). The reported outcomes of these studies show that the FREIs have had suitable mechanical properties to be used as seismic isolators (Toopchi-Nehzad et al. 2011).

Despite all beneficial characteristics of bonded and un-bonded carbon FREIs (CFREIs), concerns still exist about their efficiency and implementation. In an unbonded FREI, the isolator is placed between the sub and superstructure supports without any bonding or fastening at its contact surfaces. During an earthquake, the shear loads at the contact surfaces of an un-bonded isolator are to be transferred through friction only, this makes unbonded FREIs susceptible to slip under certain loading conditions resulting in permanent displacements. The frictional resistance of the contact interface between the un-bonded FREI and the upper and lower supports is proportional to the compressive force. If the compressive force on an unbonded isolator approaches zero during an earthquake event, the likelihood that the shear force will exceed the friction resistance is increased (Van Engelen et. al., 2014). This can negatively affect the isolator's stability.

In a fully bonded FREI, two thick steel mounting plates are bonded to the outer rubber layers at the top and bottom of the isolator. During installation, the top and bottom mounting plates are bolted to the supper and substructure, respectively. These plates on one hand make the isolator capable of transferring the lateral shear force at the contact surfaces and on the other hand prevent the stable rollover deformation, which leads in high tensile stress demand between the fiber and elastomeric layers in the bearing's ends regions which increases the lateral stiffness of the isolator. Presence of bonded plates not only lowers the isolator's damping and isolation efficiency but also increases the production cost.

To address the aforementioned concerns and deficiencies related to bonded and un-bonded CFREIs, in this research, an innovative Elevated Semi-Bonded Carbon Fiber-Reinforced Elastomeric Isolator (ESB-CFREI) is designed and manufactured (Figure 1). Dynamic characteristics, performance and isolation efficiency of ESB-CFREI, as a cost effective seismic protection system, is investigated. The top and bottom cover plate of ESB-CFREI partially covers the CFRE bearing pad of the isolator and leaves certain pre-defined region of the bearing pad to remain not bonded while elevated a distance D from top and bottom supports as shown in Figure-2. This unique bearing's boundary condition leads the isolator to undergo lateral displacement with a new lateral deformation mechanism that differs from that of bonded and un-bonded CFREIs. Figures 2-a, b and 3-a, demonstrate the isolator's schematic, experimental and analytical (Finite Element) deformation patterns. The ESB-CFREI benefits its unique and advantageous mechanical and dynamic features from both the bonded and the un-bonded isolators, features like superior transfer of shear force due to presence of secure bolted and pinned connection to sub and supper structure supports from bonded and higher damping, isolation efficiency and cost effectiveness from the un-bonded isolator type. The experimental outcome demonstrates the beneficial dynamic characteristics of the proposed isolator.

2. Specimen Specifications and Deformation Mechanism

2.1. Specimen Specifications

A total of 12 ESB-CFREI test specimens were designed and fabricated in six identical pairs. Each ESB-CFREI pair has different Bonding Level (BL). The BL is a measure of steel-cover plate area divided by the elastomeric bearing top or bottom surface area, which varies from 37.87% to 100%. A fully bonded isolator, with top and bottom cover plates having the same size as the bearing top or bottom surface area, is denoted as a specimen with BL = 100% and is denoted as B260. Whereas, isolator with cover plates size of 160×160mm is presented with BL = 37.87% and is denoted as B160 (it should be noted that the reduced steel cover is fully bonded). 10 steel round pins with 12mm diameter provide reliable connection between the isolator's top and bottom steel cover plates and the experimental mounting supports. These pins transmit the vertical compression and lateral shear forces from the mounting supports to the isolators. All ESB-CFREIs have the same fiber reinforced elastomeric bearing pad specifications and are elevated from the top and bottom support with a clearance distance of D as shown in Figure 2.

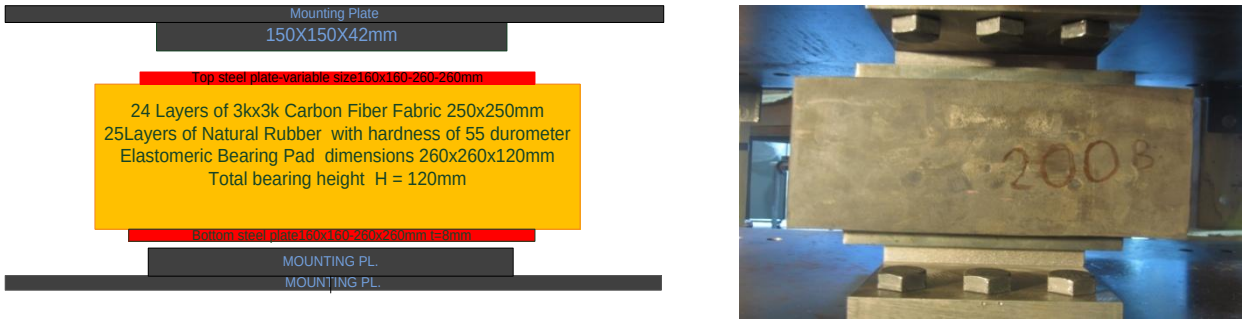

Fig. 1 - ESB-CFREI with top and bottom experimental mounting Plates (left) and Fabricated ESB-CFREI isolator (right)

The Carbon Fiber Reinforced Elastomeric Bearing Pads have dimensions of 260×260×120mm, where the bearing height H is equal to 120mm. The elastomeric material of the bearing pad is natural rubber with hardness of 55 durometer (ASTM shore-A) reinforced by 24 layers of 3k×3k carbon fiber fabric sheet of 250×250mm with average thickness of t_f = 0.22mm and elevated distance D is set to be equal 50mm.

2.2. Deformation Mechanism

To allow the un-bonded regions of the isolator's pad to move up and down freely as the isolator undergoes high lateral deformation; the CFREI's pad is designed elevated with distance D=50mm from the support base, the isolator with this specification is denoted as Elevated SB-CFREI or ESB-CFREI as shown in Figure 2a. During lateral cyclic load, the un-bonded region of the SB-CFREI's bearing pad will not be in contact with the upper and lower structural supports, therefore this new boundary condition is expected to provide the isolator with lower lateral stiffness and consequently higher isolation efficiency. The un-bonded regions of the bearing may have contact with the supporting at extreme shear strain loading, at this level of lateral deformation the isolator lateral stiffness is expected to increase due to change in deformation pattern. This phenomenon is a desirable seismic isolator's performance to achieve higher lateral stiffness at the extreme lateral deformation. The nature and magnitude of the lateral stiffness increase will be investigated in future research studies. Also in high lateral deformation some part of the bearing peels off from the steel plates as shown in experimental lateral loading Figure-2b, this partial and limited peeling-off phenomenon is allowed in order to avoid occurrence of high local peeling stress in the glued bonded zone of the bearings. Figure 2a & b show the schematic and experimental deformation mechanism of a typical ESB-CFREI isolator, and Figure 3a, b & c show the finite element deformation pattern of typical ESB-CFREI, un-bonded UB-CFREI and bonded carbon fiber reinforces elastomeric isolator and Bonded CFREI under lateral shear load.

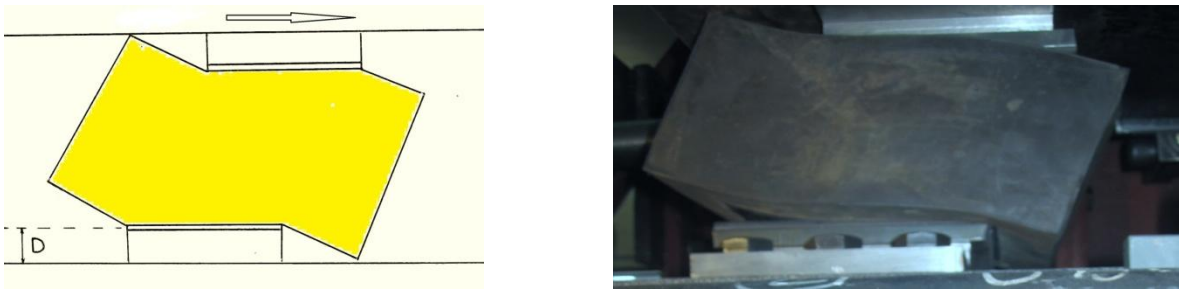

(a) (b)

Fig. 2 – Schematic (left) and experimental (right) deformation mechanism of ESB-CFREI under lateral shear load (D = distance Isolator's bearing pad is elevated from the supports)

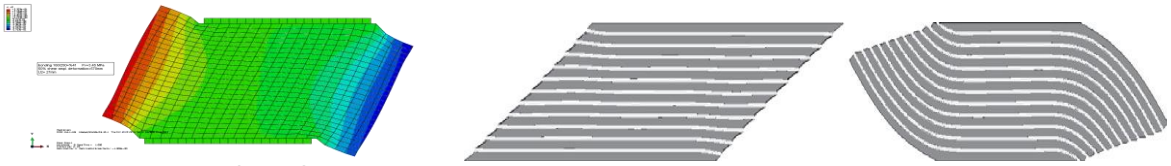

(B160) SU-CFREI (Toopchi-Nehzad et al 2010)

a - ESB-CFREI b - Bonded-CFREI c- UN-BONDED-CFREI

Fig. 3 - Laterally Deformed pattern of elevated semi-bonded, fully bonded and un-bonded CFREI (FE model)

3. Test setup, Instrumentation, and Loading Sequence

3.1. Test setup and Instrumentation

The test equipment setup was capable of applying controlled lateral displacement and axial compression load to the test specimen simultaneously. Based on experimental program requirements, efficiency and precision, dual shear test configuration was assembled for conducting the experimental program. One vertical actuator was used to apply vertical load on the top platen and a middle pull-push plate was designed to be displaced laterally by the horizontal actuator under displacement control. The vertical actuator operated under load control. Four Novotechnik model TR linear potentiometers were installed along the perimeter of the upper and lower platens to monitor the vertical displacement and two Celesco PT101 string potentiometers were installed on the push-pull platen to monitor the horizontal displacements along with those of the actuators.

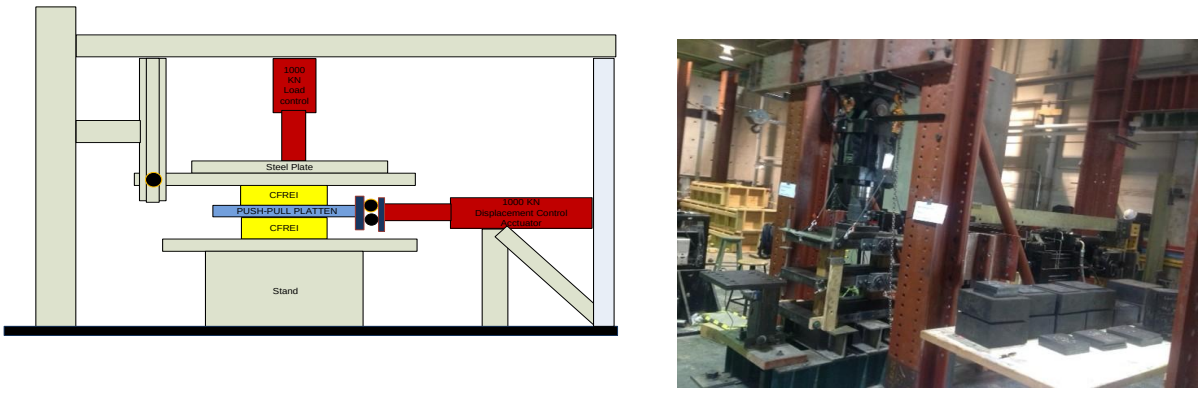

(a) schematic of dual shear test configuration (b) equipment set-up

Fig. 4 – Experimental set up

3.2. Lateral Cyclic Shear Test and input load signals

Each identical pair of component isolators were tested in a dual shear configuration under the pre-defined dynamic lateral load signals and the low frequency monotonic lateral loading, both with shear strain amplitude of 25, 50, 75, and 100%t_r. The horizontal shear tests were conducted under displacement control while the isolators were simultaneously under constant vertical compression pre- load of 250 kN. This load imposes a pressure of 3.70 MPa on bonded isolator B260 with bonding level of 100% and 9.77 MPa on component isolator B160 having the lowest bonding level of 37.87%.

The lateral shear test was conducted two times (Two Cycles) on each isolator and in each test the related lateral load-displacement hysteresis diagram was plotted in order to define the effective lateral stiffness, $K_{eff\text{-}h}$, and equivalent viscous damping ζ from both first and second test cycle. In conducting the experimental program, an average displacement rate of 57.5 mm/sec related to shear strain amplitude of %50t_r was selected for the lateral cyclic strain loading. This displacement rate is also consistent with the lateral input strain loading used by Kelly (2002) and Moon et al., (2003). All tests were repeated using a monotonic cyclic input load signal with shear strain amplitude of 100%.

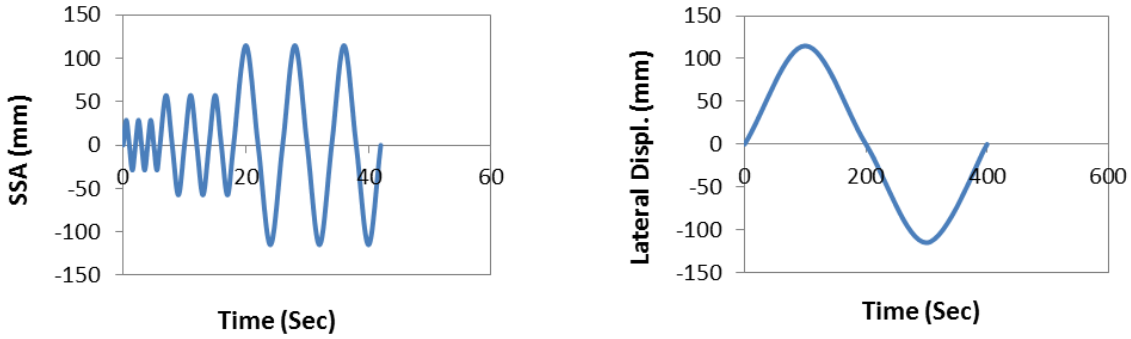

(a) dynamic lateral input Load profile (b) monotonic lateral input load signal

Fig. 5 - Lateral cyclic input load signals- (SSA = 25%, 50% & 100%t_r or 28.75, 57.5 & 115mm) under constant axial compression pre-load of Pv = 250kN)

4. Results and Discussion

4.1. SB-CFRE Lateral load-displacement hysteresis diagrams

The ESB-CFREI's force-displacement hysteretic behaviors are shown in figure 6 and the salient features of the results are summarized in Table 1. Effects of bonding variation on the isolator's dynamic characteristics are discussed in the following subsections. Further studies on the dynamic characteristics of component and compound seismic isolation system are under investigation by the author.

Table 1 – SB-CFREI Effective Lateral Stiffness K_{eff-h} and Equivalent Viscous Damping (ζ) - (Load cycles 1 and 2)

Test name and number	Isolator name	Bonding Level BL %	Axial comp. load P_v (kN)	Axial pressure σ (MPa)	Shear strain amplitude SSA %	Effective lateral stiffness, K_{eff-h} N/mm 1st cycle	Effective lateral stiffness K_{eff-h} N/mm 2nd cycle	Effective Equivalent viscous Damping 1st cycle %	Equivalent Viscous Damping 2nd cycle %
LATERAL -1 LATERAL-2	B160 B160	37.87 37.87	250 250	9.77 9.77	50 25	88.06 165.62	61.54 157.53	14.70 7.75	24.97 7.18
LATERAL-3 LATERAL-4	B180 B180	47.93 47.93	250 250	7.72 7.72	50 25	200.91 289.20	182.25 282.05	5.37 3.85	6.27 3.30
LATERAL-5 LATERAL-6	B200 B200	59.17 59.17	250 250	6.25 6.25	50 25	268.24 --------	256.78 372.87	4.89 -------	6.23 3.25
LATERAL-7 LATERAL-8	B220 B220	71.60 71.60	250 250	5.17 5.17	50 25	341.40 433.91	329.06 432.0	3.96 3.64	4.02 3.64
LATERAL-9	B220	71.60	250	5.17	75	195.57	180.02	11.53	13.00
LATERAL-10	B220	71.60	250	5.17	100	101.38	--------	27.61	----------
LATERAL-11 LATERAL-12	B 240 B240	85.21 85.21	250 250	4.34 4.34	50 25	393.28 524.42	391.55 521.88	4.76 4.69	5.21 2.72
LATERAL-13	B240	85.21	250	4.34	75	309.99	301.50	4.75	4.56
LATERAL-14	B240	85.21	250	4.34	100	216.92	196.45	8.83	10.49
LATERAL-15 LATERAL-16	B260 B260	100 100	250 250	3.69 3.69	50 25	432.59 532.43	427.08 530.69	3.36 2.26	3.42 2.85

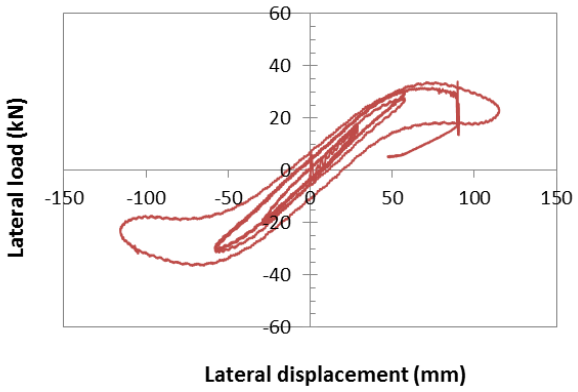

B220 Load profile б=5.17MPa and SSA=25-50-100t_r%

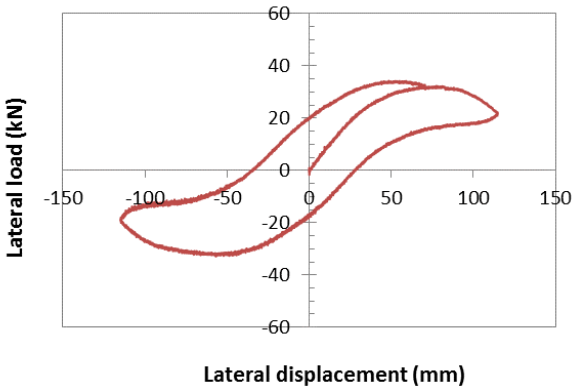

B220-SSA=100A% and б=5.17MPa

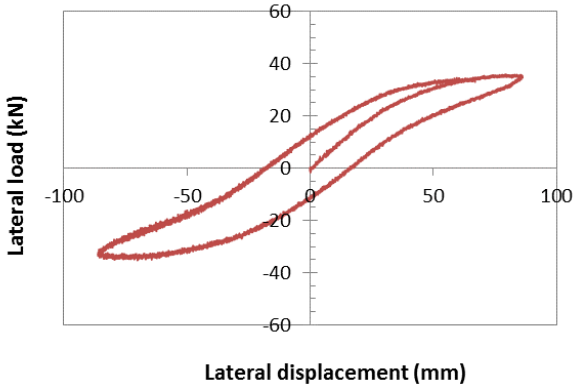

B220-SSA=%75A and б=5.17 MPa

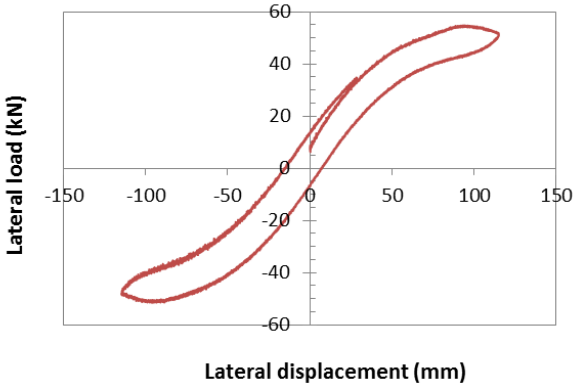

B240 SSA=%100A and б=4.34MPa

Fig. 6 - Force-Displacement Hysteresis Diagram of B220 and B240 isolators under constant pre-load of 250 KN (SSA=50-75-100%t_r)

4.2. Effect of bonding variation on dynamic characteristics of ESB-CFREI

In this section, the experimental lateral shear test results are analyzed to demonstrate the effects of bonding variation on the isolator's energy dissipation and damping, effective lateral shear stiffness and isolator's Isolation efficiencies.

4.2.1. Effect of Bonding Variation on the Isolator's Effective Lateral Stiffness

To demonstrate the effect of bonding variation on isolator's effective lateral stiffness $K_{eff\text{-}h}$, lateral shear tests were conducted on six identical pairs of ESB-CFREIs in dual shear configuration and under constant axial compression load of 250 KN. The experimentally obtained value of $K_{eff\text{-}h}$ for each isolator's type is defined and summarized in Table 1. The effective lateral shear stiffness of the isolators with different bonding level are plotted versus BL. These tests were performed at two different levels of shear strain amplitudes. Figure 7 presents the effect of bonding variation on the isolator's effective lateral stiffness at the shear strain amplitudes of 25%t_r and 50%t_r under constant vertical compression load of 250 kN. The results in Figure 7 shows that bonding variation has a considerable effect on the isolator's effective lateral stiffness, and solidly supports the idea that, as the bonding increases the isolator's effective lateral stiffness will increases. The isolator's hysteretic behavior indicates that the force-displacement curves maintains a linear trend up to shear strain amplitude of 25t_r%, as shear strain amplitude increases the lateral load-displacement curve fallows nonlinear pattern.

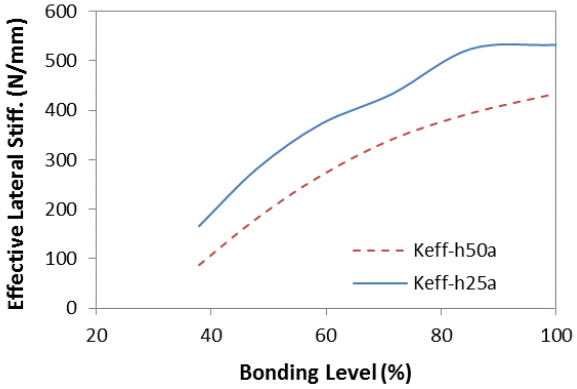

Fig. 7 - Effect of BL on the isolator effective lateral stiffness for SSA= 25 and 50%t_r PL = 250 KN

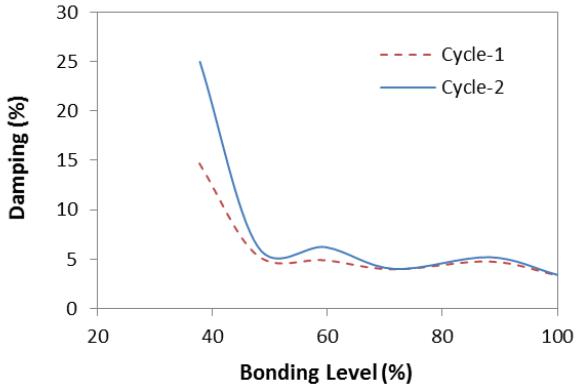

Fig. 8 - Effect of isolators BL on the lateral effective equivalent viscous damping SSA=50%t_r load cycle 1 & 2 PL = 250 KN

4.2.2. Effect of Bonding Variation on ESB-CFREI's lateral effective damping

To investigate the effect of bonding variation on the isolators effective damping, lateral cyclic shear test was conducted on each isolator's type under constant axial compression load of 250 KN. Depending on the isolator bonding, the compression pre-load imposes a pressure of 3.69 to 9.77 MPa on the isolators. For this part of study the shear strain amplitude SSA was 25% and 50% t_r for all tests. As it is demonstrated in Figure 8 and Table 1, isolators with lower level bonding like B160 have much higher effective damping in comparison with Isolator having higher bonding like B240 and B260 with BL of 85.21% and 100%, respectively. The graphs show a sharp drop of damping as the bonding varies from 37.87% to around 60%. The graph also shows that damping decreases as bonding increase to the maximum of 100%. In another words, the test results indicates that for an isolator to perform with higher level of effective equivalent viscous damping the bonding should be reduced. In general, after plotting the lateral force-displacement hysteresis diagrams and defining the related equivalent viscous damping for all tests, the outcome shows that all ESB-CFREIs at shear strain amplitude of 25-100% exhibit higher level of damping in comparison to Bonded B-CFREIs (BL=100%). Combing low bonding isolator with those of high bonding leads to compound isolator CESB-CFREIs which is expected to have higher damping. The combining technique needs more experimental investigation. At the present time the author is engaged in conducting further studies in this area.

4.2.3. Effect of shear strain level on ESB-CFREI effective lateral stiffness

To investigate the effect of shear strain amplitude on effective lateral stiffness ($K_{eff\text{-}h}$) of the ESB-CFREIs, lateral shear tests were conducted on two isolators B220 and B240 under a constant compression load of 250 KN. Each isolator was imposed to cyclic shear loading with shear strain amplitude of γ = 25, 50, 75 and 100t_r%. The lateral load-displacement hysteresis diagram of both isolators were defined and plotted for all input lateral loading. At each shear strain amplitude the linear effective lateral stiffness Keff-$h_{(\gamma)}$ was defined. Therefore all the values of Keff-h related to each isolator under four levels of shear strain loading were defined and calculated according to the equation (1) recommended by ASCE and FEMA.

$$\mathbf{K}_{eff\text{-}h(\gamma)} = \frac{|\boldsymbol{F}max|+|\boldsymbol{F}min|}{|\boldsymbol{D}max|+|\boldsymbol{D}min|} \qquad (1)$$

where ***F****max* and ***F****min* are the maximum positive and maximum negative force on the force-displacement hysteresis diagram related to maximum positive and maximum negative displacement ***D****max* and ***D****min,* respectively, for the specific loading cycle. This stiffness is interpreted as the effective or overall stiffness of the bearing and is used to calculate the stored or elastic energy of the isolator during each test complete loading cyclic. Figure 9 shows effect of shear strain amplitude on the effective lateral stiffness of the ESB-CFREIs under constant compression load of 250 KN (B220 & B240 Isolators)

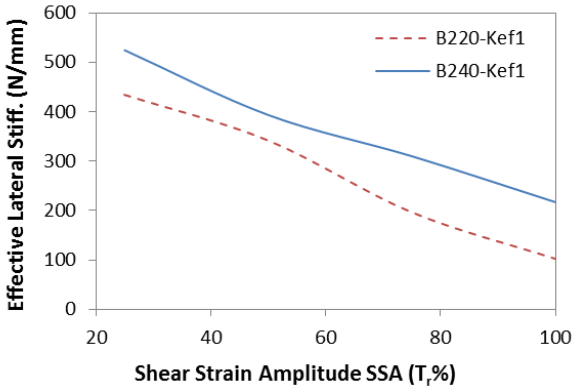

Fig. 9 - Effect of shear strain amplitude on the effective lateral stiffness of the ESB-CFREIs under constant compression load of 250 KN (B220 & B240 Isolators)

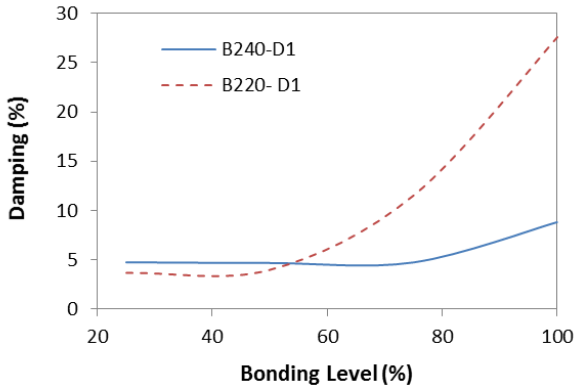

Fig. 10 - Effect of isolator's shear strain amplitude variation on the equivalent viscous damping under constant compression load of 250 KN (B220 & B240 isolators)

4.2.4. Effect of shear strain amplitude variation on the ESB-CFREI effective equivalent viscous damping

The effective lateral equivalent viscous damping of the isolators with respect to shear strain amplitude was investigated and is demonstrated in Table 1. For component isolators B220 and B 240 the load-displacement hysteresis diagrams for shear strain amplitudes of 25, 50, 75 and 100t_r% under constant axial compression load of 250 KN are defined and the experimental results are plotted. The force-displacement hysteresis diagram for isolator B220 and B240 are plotted in Figure 6. Effect of isolator's shear strain amplitude variation on the equivalent viscous damping under constant compression load of 250 KN (B220 & B240 isolators are shown in Figure-10

4.2.5. ESB-CFREI damping characteristics

Kelly (1999) stated that curvature in the fiber reinforcing sheets due to the bearing deformation causes individual fiber strands to slip against each other leading to additional energy dissipation in the bearing. Due to unique deformation mechanism of the ESB-CFREIs (Figure 2) under high lateral strain load, the fiber reinforcement layers experience higher curvature. At high shear strain amplitude the un-bonded regions of the CFRE bearing pad moves up and down in vertical direction and causes the fiber strands

not only to slip against the surrounding rubber layers in higher extend but also makes the fiber strands to slip and rub against each other with higher magnitude leading to greater values of damping. The test outcome supports this postulate and shows greater isolator's damping when compared with Bonded CFREIs (BL of 100%). Nevertheless, the unbonded regions of ESB-CFREI's bearing with lower level of bonding undergo higher vertical deformation making the fiber strand to experience higher curvature, consequently higher magnitude of damping. Table 1 display the isolator's damping values indicating higher damping values for isolators with lower bonding.

4.2.6. ESB-Isolator Effective Compression Stiffness K_{eff-v} and Modulus E_c

Axial compression cyclic tests were conducted on all ESB-CFREI's with different bonding level under load control at two different pre-load magnitudes of 116 and 233 KN. In the first phase of the tests specimens were slowly loaded up to PL1 = 116 KN vertical pre-load, and then continued with three fully reversed load cycles of amplitude ±25PL1%, at the final stage the specimens were monotonically unloaded in a similar way. The loading and un-loading process was repeated for the higher pre-load of PL2 = 233KN. The isolator's effective axial compression stiffness K_{eff-v} and modulus at lower and higher values of axial loads are defined in Table 2. Depending on the bonding level the isolators experienced pressure of 2.15 to maximum of 11.38 MPa due to the lower and higher loading level respectively.

Table 2 – ESB-CFREI's Isolation efficiency, effective compression stiffness and compression modulus

TEST	TEST NAME	Isolator type	Bonding Level %	Axial Comp. Pre-Load Pv KN	Max. Axial Comp. Stress б MPa	AVARAGE K_{eff-v} kN/mm LVDTs & ACT.	Effective Comp. Modulus E_C MPa	Isolation efficiency K_v/K_h
1	VERTICAL	B-160	37.87	116	5.66	98.45	172.12	1058
2	VERTICAL	B160	37.87	233	11.38	104.95	193.11	1243
3	VERTICAL	B180	47.93	116	4.48	109.43	201.35	588
4	VERTICAL	B180	47.93	233	9.00	120.10	220.80	645
5	VERTICAL	B200	59.17	116	3.63	131.58	242.11	486
6	VERTICAL	B200	59.17	233	7.28	137.10	252.26	527
7	VERTICAL	B220	71.60	116	3.00	138.10	254.10	411
8	VERTICAL	B220	71.60	233	6.02	142.07	261.41	423
9	VERTICAL	B240	85.21	116	2.52	152.63	280.84	397
10	VERTICAL	B240	85.21	233	5.06	157.43	289.74	410
11	VERTICAL	B260	100	116	2.15	145.18	217.78	278
12	VERTICAL	B260	100	233	4.31	144.00	264.96	338

5. Conclusion

The experimental findings and achievements to date can be summarized as follows:

- Increase in bonding level BL will increase the ESB-CFREI's effective axial compression stiffness and modulus.
- All isolators with different level of bonding undergone axial compression stress of 4.31 to 11.38 MPa induced from constant compression pre-load and maximum cyclic loading respectively. All isolator while resisting simultaneous lateral deformation demonstrated satisfactory performance. After completion of tests no delaminating damage was detected.
- Isolators with lower bonding level demonstrate higher equivalent viscous damping. For example as indicated in table T-1 the B220 isolator under shear strain loading of SSA= %100 isolate with equivalent viscous damping of % 27.76, while the B240 isolator exhibits a damping of % 8.83 and %10.49 for 1st and 2nd loading cycle at the same shear strain amplitude.
- Test out comes indicates Increase in isolators bonding level reduces its effective lateral stiffness.

- ESB-CFREIs have higher effective lateral stiffness at lower level of shear strain amplitude and it reduces as Shear Strain Amplitude SSA increases.
- Isolator's equivalent viscous damping will increases at higher shear strain amplitude, the increasing pattern differs for isolators with different bonding level. Figure 10a and 10b demonstrate the desirable damping increase as isolators undergo higher shear strain loading.
- Plots of Damping Vs Bonding level of the ESB-CFREIs indicates that isolators with low bonding level have higher damping and energy dissipation capability.
- It is suggested that with further research and development ESB-CFREI could be implemented as low cost seismic isolators with sufficient isolation efficiency and damping.

6. Acknowledgements

The Earthquake Engineering Research Facility EERF of the University of British Columbia (UBC) provided the financial and technical support for conducting this research.

7. References

ASHKEZARIA, G.H., AGHAKOUCHAKA, A.A. DEHGHANI M.K. Design, manufacturing and evaluation of the performance of steel like fiber reinforced elastomeric seismic isolators. *J Mater Process Technol*, Vol. 197, No. 1–3, 2008, pp. 140–150.

KELLY, J.M. *Earthquake-Resistant Design with Rubber*. 2nd ed. London: Springer; 1997.

KELLY, J.M. Analysis of fiber-reinforced elastomeric isolators *J Seismol Earthq Engineering*, Vol. 2, No. 1, 1999, pp. 19–34.

KELLY, J.M. Seismic isolation systems for developing countries. *Earthquake Spectra*, Vol. 18, No. 3, 2002, pp. 385–406.

NAGHSHINEH, A.K., AKYÜZ, U., CANER, A. Comparison of fundamental properties of new types of fiber-mesh reinforced seismic isolators with conventional isolators, *Earthquake Engineering Structural Dynamics*, Vol. 43, No. 2, 2014, pp. 301–316.

KANG, B.S., KANG, G.J., MOON, B.Y. Hole and lead plug effect on fiber reinforced elastomeric isolator for seismic isolation. *J Mater Process Technol*, Vol. 140, 2003, pp. 592–597.

TOOPCHI-NEZHAD, H., DRYSDALE, R.G., TAIT, M.J. Parametric study on the response of stable unbonded fiber-reinforced elastomeric isolators (SU-FREIs). *J Compos Mater*, Vol. 43, No. 15, 2009, pp. 1569–1587.

TOOPCHI-NEHZAD H, TAIT MJ, DRYSDALE R G, Bonded versus unbonded strip fiber-reinforced elastomeric isolators: finite element analysis. *Composite Structures* 2011; 93:850–859.

MOON, B.Y., KANG G.J., KANG, B.S., KELLY, J.M. Design and manufacturing of fiber reinforced elastomeric isolator for seismic isolation. *J Mater Process Technol*, Vol. 130, No. 131, 2002, 145–50.

MORDINI, A., STRAUSS, A. An innovative earthquake isolation system using fibre reinforced rubber bearings. *Engineering Structures*, Vol. 30, No. 10, 2008, pp. 2739–2751.

NAEIM, F., KELLY, J.M. *Design of Seismic Isolated Structures: From Theory to Practice*. John Wiley & Sons, Inc.: New York, 1999.

VAN ENGELEN, N., C. OSGOOEI, P.M., TAIT, M.J. and KONSTANTINIDIS, D. Partially bonded fiber-reinforced elastomeric isolators (PB-FREIs) Struct. Control Health Monit. (2014) DOI: 10.1002/stc.1682.